Polarized emission of quantum dots in microcavity and anisotropic Purcell factors

Yi-Shan Lee and Sheng-Di Lin*

Department of Electronics Engineering, National Chiao Tung University, 1001 University Road, Hsinchu 30010, Taiwan

sdlin@mail.nctu.edu.tw

Abstract: We study the polarization properties of quantum dot (QD) emission coupled with the fundamental cavity modes. A rotation of polarization axis and a change of polarization degree are observed as the coupling is varied. To explain this observation, we derive an analytical model considering the polarization misalignment between QD dipole and cavity mode field. Our model also provides a new approach to extract the anisotropic Purcell factors by analyzing the polarization of detected quantum dot emission coupled to the cavity mode, which paves the way to develop high-efficiency polarized single photon sources.

OCIS codes: (140.3945) Microcavities; (160.4760) Optical properties.

References and links

1. J. M. Gérard and B. Gayral, "InAs quantum dots-artificial atoms for solid-state cavity-quantum electrodynamics," Physica E **9**(1), 131–139 (2001).
2. J. M. Gerard and B. Gayral, "Strong Purcell effect for InAs quantum boxes in three-dimensional solid-state microcavities," J. Lightwave Technol. **17**(11), 2089–2095 (1999).
3. T. Yoshie, A. Scherer, J. Hendrickson, G. Khitrova, H. M. Gibbs, G. Rupper, C. Ell, O. B. Shchekin, and D. G. Deppe, "Vacuum Rabi splitting with a single quantum dot in a photonic crystal nanocavity," Nature **432**(7014), 200–203 (2004).
4. J. P. Reithmaier, G. Sek, A. Löffler, C. Hofmann, S. Kuhn, S. Reitzenstein, L. V. Keldysh, V. D. Kulakovskii, T. L. Reinecke, and A. Forchel, "Strong coupling in a single quantum dot-semiconductor microcavity system," Nature **432**(7014), 197–200 (2004).
5. P. Michler, A. Kiraz, C. Becher, W. V. Schoenfeld, P. M. Petroff, L. Zhang, E. Hu, and A. Imamoglu, "A quantum dot single-photon turnstile device," Science **290**(5500), 2282–2285 (2000).
6. A. Kiraz, M. Atature, and A. Imamoglu, "Quantum-dot single-photon sources: Prospects for applications in linear optics quantum-information processing," Phys. Rev. A **69**(3), 032305 (2004).
7. G. S. Solomon, M. Pelton, and Y. Yamamoto, "Single-mode spontaneous emission from a single quantum dot in a three-dimensional microcavity," Phys. Rev. Lett. **86**(17), 3903–3906 (2001).
8. M. Pelton, C. Santori, J. Vucković, B. Zhang, G. S. Solomon, J. Plant, and Y. Yamamoto, "Efficient source of single photons: a single quantum dot in a micropost microcavity," Phys. Rev. Lett. **89**(23), 233602 (2002).
9. C. Santori, D. Fattal, J. Vucković, G. S. Solomon, and Y. Yamamoto, "Indistinguishable photons from a single-photon device," Nature **419**(6907), 594–597 (2002).
10. N. Gisin, G. Ribordy, W. Tittel, and H. Zbinden, "Quantum cryptography," Rev. Mod. Phys. **74**(1), 145–195 (2002).
11. T. Heindel, C. A. Kessler, M. Rau, C. Schneider, M. Fürst, F. Hargart, W.-M. Schulz, M. Eichfelder, R. Roßbach, S. Nauerth, M. Lermer, H. Weier, M. Jetter, M. Kamp, S. Reitzenstein, S. Höfling, P. Michler, H. Weinfurter, and A. Forchel, "Quantum key distribution using quantum dot single-photon emitting diodes in the red and near infrared spectral range," New J. Phys. **14**(8), 083001 (2012).
12. E. Knill, R. Laflamme, and G. J. Milburn, "A scheme for efficient quantum computation with linear optics," Nature **409**(6816), 46–52 (2001).
13. B. Gayral, J. M. Gerard, B. Legrand, E. Costard, and V. Thierry-Mieg, "Optical study of GaAs/AlAs pillar microcavities with elliptical cross section," Appl. Phys. Lett. **72**(12), 1421–1423 (1998).
14. A. Daraei, A. Tahraoui, D. Sanvitto, J. A. Timpson, P. W. Fry, M. Hopkinson, P. S. S. Guimaraes, H. Vinck, D. M. Whittaker, M. S. Skolnick, and A. M. Fox, "Control of polarized single quantum dot emission in high-quality-factor microcavity pillars," Appl. Phys. Lett. **88**(5), 051113 (2006).
15. A. Daraei, D. Sanvitto, J. A. Timpson, A. M. Fox, D. M. Whittaker, M. S. Skolnick, P. S. S. Guimaraes, H. Vinck, A. Tahraoui, P. W. Fry, S. L. Liew, and M. Hopkinson, "Control of polarization and mode mapping of small volume high Q micropillars," J. Appl. Phys. **102**(4), 043105 (2007).
16. J. M. Gérard, B. Sermage, B. Gayral, B. Legrand, E. Costard, and V. Thierry-Mieg, "Enhanced spontaneous emission by quantum boxes in a monolithic optical microcavity," Phys. Rev. Lett. **81**(5), 1110–1113 (1998).

#200956 - $15.00 USD Received 7 Nov 2013; revised 30 Dec 2013; accepted 10 Jan 2014; published 15 Jan 2014

17. C. Böckler, S. Reitzenstein, C. Kistner, R. Debusmann, A. Loffler, T. Kida, S. Hofling, A. Forchel, L. Grenouillet, J. Claudon, and J. M. Gerard, "Electrically driven high-Q quantum dot-micropillar cavities," Appl. Phys. Lett. **92**(9), 091107 (2008).
18. A. Dousse, L. Lanco, J. Suffczyński, E. Semenova, A. Miard, A. Lemaître, I. Sagnes, C. Roblin, J. Bloch, and P. Senellart, "Controlled light-matter coupling for a single quantum dot embedded in a pillar microcavity using far-field optical lithography," Phys. Rev. Lett. **101**(26), 267404 (2008).
19. I. Favero, G. Cassabois, C. Voisin, C. Delalande, Ph. Roussignol, R. Ferreira, C. Couteau, J. P. Poizat, and J. M. Gerard, "Fast exciton spin relaxation in single quantum dots," Phys. Rev. B **71**(23), 233304 (2005).
20. I. Favero, G. Cassabois, A. Jankovic, R. Ferreira, D. Darson, C. Voisin, C. Delalande, Ph. Roussignol, A. Badolato, P. M. Petroff, and J. M. Gerard, "Giant optical anisotropy in a single InAs quantum dot in a very dilute quantum-dot ensemble," Appl. Phys. Lett. **86**(4), 041904 (2005).
21. D. N. Krizhanovskii, A. Ebbens, A. I. Tartakovskii, F. Pulizzi, T. Wright, M. S. Skolnick, and M. Hopkinson, "Individual neutral and charged $In_xGa_{1-x}As$-GaAs quantum dots with strong in-plane optical anisotropy," Phys. Rev. B **72**(16), 161312 (2005).
22. C. H. Lin, W. T. You, H. Y. Chou, S. J. Cheng, S. D. Lin, and W. H. Chang, "Anticorrelation between the splitting and polarization of the exciton fine structure in single self-assembled InAs/GaAs quantum dots," Phys. Rev. B **83**(7), 075317 (2011).
23. S. Ohno, S. Adachi, R. Kaji, S. Muto, and H. Sasakura, "Optical anisotropy and photoluminescence polarization in single InAlAs quantum dots," Appl. Phys. Lett. **98**(16), 161912 (2011).
24. C. Tonin, R. Hostein, V. Voliotis, R. Grousson, A. Lemaitre, and A. Martinez, "Polarization properties of excitonic qubits in single self-assembled quantum dots," Phys. Rev. B **85**(15), 155303 (2012).
25. M. Munsch, A. Mosset, A. Auffeves, S. Seidelin, J. P. Poizat, J.-M. Gérard, A. Lemaître, I. Sagnes, and P. Senellart, "Continuous wave versus time-resolved measurements of Purcell factors for quantum dots in semiconductor microcavities," Phys. Rev. B **80**(11), 115312 (2009).
26. T. Tawara, H. Kamada, S. Hughes, H. Okamoto, M. Notomi, and T. Sogawa, "Cavity mode emission in weakly coupled quantum dot--cavity systems," Opt. Express **17**(8), 6643–6654 (2009).

1. Introduction

The system of single semiconductor quantum dots (QDs) coupled to cavities paves the way for the exploration of cavity quantum electrodynamics (CQED) effects [1]. In the past decade, many CQED phenomena in such systems, including Purcell effect in the weak coupling regime [2] as well as the vacuum Rabi splitting in the strong coupling regime [3,4], have been performed and investigated extensively due to their potential applications in quantum information science [5,6]. Weak exciton-photon coupling reveals a pronounced modulation on the spontaneous emission (SE) rate of the QDs through the Purcell effect [7]. The magnitude of modulation, namely, the ratio between the QD's SE rate with $(1/\tau_{cav})$ and without $(1/\tau_0)$ cavity can be quantified by the following expression:

$$F = \frac{\tau_0}{\tau_{cav}} = \frac{3Q(\lambda_c/n)^3}{4\pi^2 V_{eff}} \cdot L(\Delta) \cdot \frac{\left|\vec{\varepsilon}(\vec{r})\right|^2}{\left|\vec{\varepsilon}_{\max}\right|^2} \cdot \left(\frac{\vec{d} \cdot \vec{\varepsilon}(\vec{r})}{\left|\vec{d}\right| \cdot \left|\vec{\varepsilon}(\vec{r})\right|} \right)^2, \tag{1}$$

where the first of the four terms on the right side takes on the value denoted F_P. Q is the quality factor of cavity mode, V_{eff} is the effective mode volume, and λ_c is the wavelength of cavity mode. Moreover, $L(\Delta) = \delta\omega_c^2 \big/ \left(\delta\omega_c^2 + 4\Delta^2\right)$ is a Lorentz function of cavity linewidth $\delta\omega_c$ and a function of detuning Δ. The last two terms are the mismatches between dipole and field in the space and polarization, respectively.

Micropillars, owing to its directional radiation pattern, exhibit a high extraction efficiency of photons and thus become a promising candidate for accomplishing efficient single photon devices [8] and further for generating indistinguishable photons [9], where those are at the basis of quantum cryptography [10,11]. The single photons with specific polarization are often used to encode qubit information in quantum computation and cryptography [10,12]. On the other hand, single photon source with variable polarization are quite appealing for avoiding the loss caused by external polarization-resolved components. To control the polarization properties of emitted photons, an anisotropic geometry is introduced to the micropillars [13]. Such an anisotropic cross section lifts the twofold degeneracy of fundamental modes into a pair of linearly polarized modes. A continuous polarization control of single QD emission has been achieved by changing the coupling of QD with the cavity

#200956 - $15.00 USD Received 7 Nov 2013; revised 30 Dec 2013; accepted 10 Jan 2014; published 15 Jan 2014

mode (CM) [14,15]. However, a complete experiment/model of the polarization properties, such as the polarization degrees and angles, of QD emission controlled by the Purcell effect is still absent.

In this paper, we investigated the polarization-resolved spectroscopy of the QD emission coupled to the CM, both experimentally and theoretically. In experiment, the polarization axis of QD emission is continuously changed with the detuning between QD and CM, as well as the polarization degree. An analytical model considering the coupling between two cavity modes and the exciton state has been proposed to quantitatively explain not only our observations on QDs' polarization behavior but also those in the previous reports [14,15]. Moreover, since the Purcell factor is a figure of merit for characterizing cavity-based single photon devices, developing a reliable approach to extract the Purcell factor is requisite and various methods have been demonstrated previously. The most intuitive way to probe the Purcell effect is to directly employ Eq. (1). By comparing the QD lifetime at and far from resonance with the cavity mode, the Purcell factor can be determined [16]. There are other signatures reflecting the Purcell effect. For example, as the SE of the QD exciton becomes faster near resonance due to the Purcell effect, the pump power required to saturate the optical transitions will be increased. The faster emission rate also enhances the emission intensity at saturation. Therefore, measuring the pump rate where the QD emission intensity saturates [2] or the QD emission intensity at saturation [17,18] could quantitatively illustrate the Purcell effect. Alternatively, by measuring the polarization-resolved emission of QDs, we provide a new approach for extracting the anisotropic Purcell factors of the microcavity.

2. Experimental method, results and discussions

The sample studied in this work is fabricated from a planar microcavity grown by molecular beam epitaxy. The microcavity consists of a one λ GaAs cavity surrounded by alternating AlAs and GaAs layers of 24/20 pairs as the bottom/top distributed Bragg reflector (DBR). One layer of InAs QDs is grown at the antinode of cavity and the area density of QDs is approximately 1×10^9 cm^{-2}. The pillars are fabricated first by conventional lithography using negative photoresist (AZ 5214E) and following by the inductively coupled plasma (ICP) etching. The photoresist (PR) is then patterned into groups of circles by photo-lithography and serves as a mask in the following chloride-based ICP etching. After etching and defining the pillars, the residual PR is removed by O_2 plasma ashing. A scanning electron micrograph (SEM) of pillar with diameter of 3 μm is shown in the inset of Fig. 1. Emission spectra are taken in a low-temperature micro-photoluminescence (μ-PL) setup. A 632.8nm line of HeNe laser is focused onto the pillars through an objective lens with a numerical aperture (NA) of 0.5. The PL signals are analyzed by a spectrometer consisting of a 0.55-m monochromator and a liquid-nitrogen-cooled charge-coupled detector (CCD) camera, which provides a spectral resolution of 80 μeV. The polarization-resolved μ-PL is accomplished with the mounting of a rotating half-wave plate and a fixed linear polarizer in front of the monochromator. All the following data are taken with a half-waveplate rotating in the steps of 3° from 0° to 180°such that the PL intensity of the whole polarization plane can be mapped. By applying this polarization-resolved spectroscopy, we can also analyze the fine structure splitting of exciton with an accuracy of 5μeV.

#200956 - $15.00 USD Received 7 Nov 2013; revised 30 Dec 2013; accepted 10 Jan 2014; published 15 Jan 2014

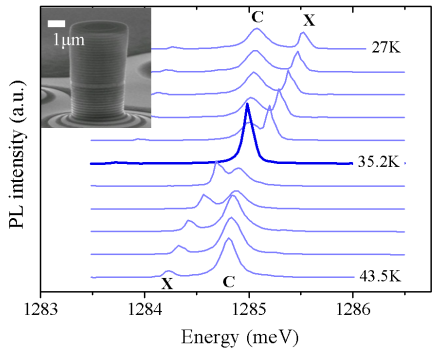

Fig. 1. Temperature-dependent QD emission spectra of a 3-μm diameter micropillar. Resonance between QD and CM is observed at T = 35.2 K. The inset shows a SEM picture of the studied micropillar.

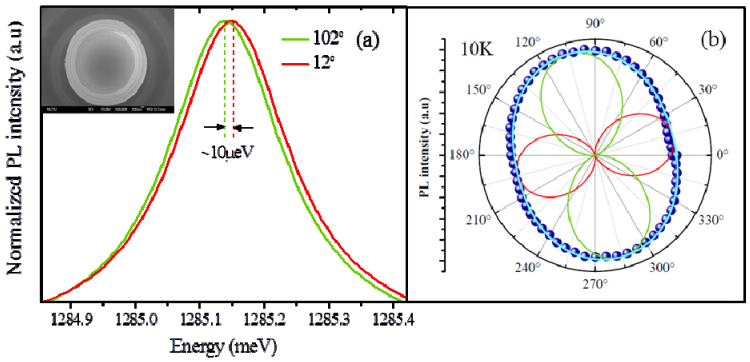

Fig. 2. (a) Normalized PL of CM taken at two polarization angles showing that the splitting between two linearly polarized modes is about 10 μeV. There is slight difference in the quality factors of two cavity modes. Inset: SEM picture of top-viewed micropillar. (b) Polarization polar diagram of measured total PL intensity (blue dots) for CM at T = 10K. The green and red lines represent respectively two orthogonal linearly-polarized modes with polarization angle of 102° and 12°.

Temperature-dependent PL spectra from the studied 3-μm-diameter micropillar with quality factor Q = 7,600 are recorded in Fig. 1. To obtain an authentic quality factor, we excite the pillar with high pump power for feeding a broad and smooth background sources to the cavity. The estimated maximal Purcell factor F_P is 14 for the studied micropillar with V_{eff} = 0.87 μm^3. By varying the temperature, we can control the coupling of the QD with the CM. The energy state of the QD is brought into resonance with the CM at T = 35.2 K and the Purcell enhancement results a pronounced increase in the PL intensity at resonance. The energy crossing at resonance indicates a weak coupling regime for this QD-microcavity system.

The fundamental cavity mode HE_{11} of circular micropillars is twofold polarization degenerate. However, this degeneracy is lifted due to a slight asymmetry (with ellipticity~0.02, referring to the inset of Fig. 2(a)) in the cross section of the studied micropillar, which is caused during the fabrication process [13]. The energy splitting between the two linearly polarized modes of our pillar is about 10 μeV as shown in Fig. 2(a). The polarization angles of these two linearly polarized modes are determined by measuring the emission intensity in the whole polarization plane. As shown in Fig. 2(b), one of the split modes is polarized along 102° and emits stronger PL intensity than the perpendicular one. Above measurements are performed at T = 10 K.

#200956 - $15.00 USD Received 7 Nov 2013; revised 30 Dec 2013; accepted 10 Jan 2014; published 15 Jan 2014

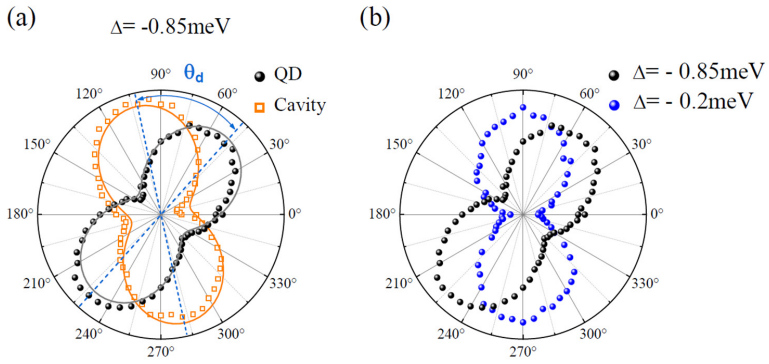

Fig. 3. (a) Polarization polar diagram of QD (black dot) and CM (orange square) for $\Delta = -0.85$ meV. θ_d is the included angle between the polarization angles of QD and CM. (b) Polarization diagram of QD for $\Delta = -0.85$ meV (black dot) and –0.2meV (blue dot).

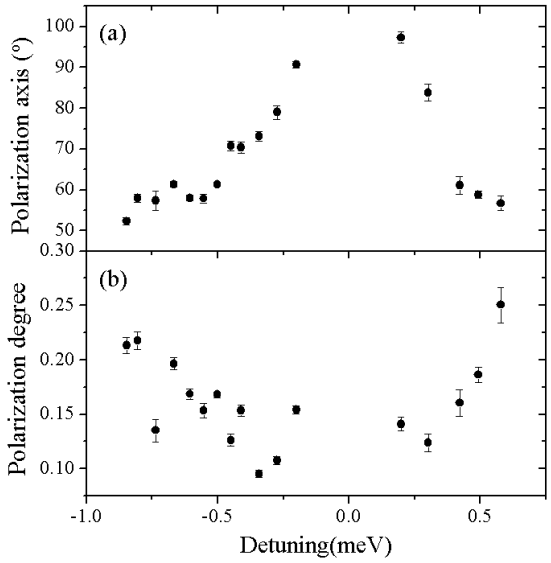

Fig. 4. (a) Polarization axis and (b) polarization degree of detected QD emission as a function of detuning.

For the target spectral line of the QD in Fig. 1, we cannot confidently identify it as an exciton or a charged exciton since it has no observable fine structure splitting. As shown in Fig. 3(a), the polarization of its emission intensity is measured at T = 10 K. We have observed a certain degree of polarization up to 0.2. Such polarization anisotropy was found to vary from dot to dot and ranged from 0 to 0.5 in our sample. Similar observations were reported previously by other groups for InAs or InGaAs QDs [19–22]. Besides, from the investigations of polarization anisotropy on tens of individual QDs, we found that the polarization axes were not aligned along the crystallographic axes. The optical anisotropy misaligned with respect to the crystallographic axes is attributed to the strong valence-band mixing which is due to the shape and strain anisotropies [23,24].

We show the polarization orientations of the QD and of the CM at detuning $\Delta = -0.85$ meV together in Fig. 3(a). An included angle θ_d exists between the polarization plane of the QD and the CM. Under the detuning $\Delta = -0.85$ meV and $\Delta = -0.2$ meV, we observed a change in the polarization direction as shown in Fig. 3(b). We thus depict the polarization axis and the polarization degree of QD emission as a function of detuning in Fig. 4. As seen in

#200956 - $15.00 USD Received 7 Nov 2013; revised 30 Dec 2013; accepted 10 Jan 2014; published 15 Jan 2014

Figs. 4(a) and 4(b), both the polarization axis and the polarization degree change with the detuning. According to Eq. (1), it is expected that the misalignment between the polarization axis of QD and CM could play a role in the observed change of polarization. Thus a model which takes the misalignment between the QD and the CM into consideration is needed to quantitatively explain this observation.

3. Theory for anisotropic Purcell effect

To illustrate the polarization-dependent Purcell effect, an analytical model is derived as follows. When the QD is pumped with a pumping rate r, it emits photons via either cavity mode or leaky modes. The SE rate of exciton coupled with the leaky modes is denoted γ_x. In addition, the exciton emission rate coupled to the cavity mode is modified by the Purcell effect and can be expressed as $\Gamma = \gamma_X F_{eff} L(\Delta)$, where F_{eff} denotes the effective Purcell factor taking the spatial and polarization mismatch between the dipole and the mode field into account. The photons emitting from cavity and leaky modes are then collected by the polarization-resolved μ-PL setup. The PL intensity from desired QD collected by the detector can be given by [25]

$$I_{QD}^{\det}(\Delta, r, \theta) = I_{QD}^{leak}(\Delta, r, \theta) + I_{QD}^{cav}(\Delta, r, \theta), \quad (2)$$

where we assume that the QD emission comes from the exciton consisting of a singlet state. The PL intensity is a function of detuning Δ, pumping rate r and analyzer axis θ. The efficiencies of cavity mode and leaky mode coupled to the detector are denoted η_{leak} and η_{cav}, respectively. The PL of the QD emitted through the leaky mode keeps its polarization properties [23] and has the expression of

$$I_{QD}^{leak}(\Delta, r, \theta) = \mathrm{A}^{-1}\eta_{leak}\gamma_X p_X(\Delta, r)\left[1 + N\cos^2(\theta - \theta_D)\right], \quad (3)$$

where A is the intensity integral over the whole polarization plane and given as (2 + N)π. N is a parameter depending on the linear polarization degree of the QD. $N = 2P_l/(1-P_l)$ if the polarization degree of the QD emission is P_l. θ_D is the direction of polarization anisotropy. p_X is the steady excitonic population and can be derived from the rate equations, which depends on detuning Δ and pumping rate *r* but not on analyzer axis θ. The PL from the cavity mode is

$$I_{QD}^{cav}(\Delta, r, \theta) = B^{-1}\eta_{cav} p_X(\Delta, r)\Gamma = B^{-1}\eta_{cav} p_X(\Delta, r)\gamma_X F\cos^2(\theta - \theta_C)L(\Delta), \quad (4)$$

where B is again the intensity integral over the whole polarization plane but given as π. In order to investigate the impact of misalignment between the QD and the CM on the PL, the inner product of the dipole and field orientation is separated from the effective Purcell factor and is given with a function of $\cos^2(\theta-\theta_c)$, where θ_c is the polarization angle of single cavity mode. By doing this, we have $F_{eff} = F\cos^2(\theta-\theta_c)$. F is the Purcell factor involving only the spatial mismatch. This expression manifests that the Purcell effect selectively enhances the SE rate of photons of the same polarization. When the analyzer axis is chosen to align along the CM, the effective Purcell factor arrives at a maximum so that the detected PL intensity along this axis is greatly contributed from the photons emitted into the CM. On the contrary, zero effective Purcell factor occurs at the direction perpendicular to the CM, which leads to a leaky mode dominated PL intensity. By putting Eqs. (3) and (4) into Eq. (2), the detected PL intensity can be written in the following formula:

$$I_{QD}^{\det}(\Delta, r, \theta) = \pi\eta_{leak}\gamma_X p_X\left[\frac{1 - P_l}{2} + P_l\cos^2(\theta - \theta_D) + \alpha F\cos^2(\theta - \theta_C)L(\Delta)\right], \quad (5)$$

where $\alpha = \eta_{cav}/\eta_{leak}$. All the terms related to N have been replaced with P_l. To illustrate the Purcell effect on the polarization properties of detected PL described by Eq. (5), we plot the

#200956 - $15.00 USD Received 7 Nov 2013; revised 30 Dec 2013; accepted 10 Jan 2014; published 15 Jan 2014

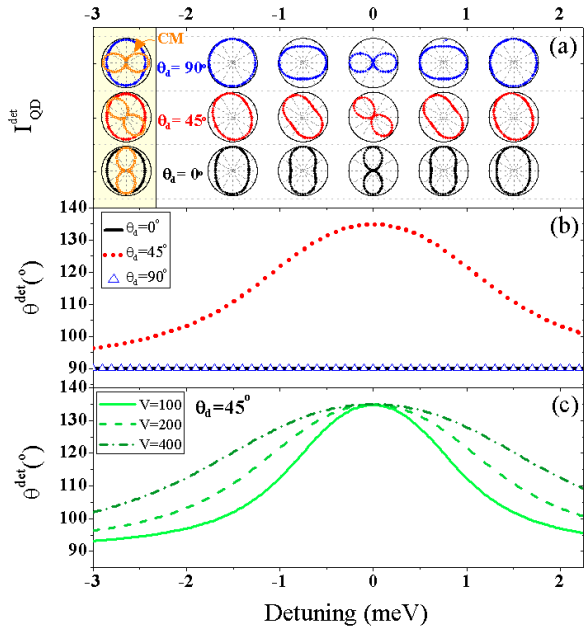

Fig. 5. (a) Detected emission intensity in the polar diagram and (b) polarization axis of detected PL for θ_d = 0°(black symbol), 45°(red symbol) and 90°(blue symbol) as a function of detuning. The polar diagrams plotted with orange symbol in (a) represent the CM polarized at 90°, 135° and 180° respectively. (c) The curves of polarization axis as a function of detuning for different magnitudes of V when θ_d = 45°.

PL intensity of QD coupled to single mode in a polar diagram by letting αF = 20 as shown in Fig. 5(a) for θ_d = 0°, 45° and 90° at several detunings, where $\theta_d = \theta_C - \theta_D$. Here we consider a QD which has a polarization degree of 0.1 at large detuning (off resonance). For each included angle, the polarization degree is modified as the coupling of QD with CM is changed and reaches a maximum at resonance, where the polarization degree of detected PL is defined by $(I_{max}-I_{min})/(I_{max}+I_{min})$.What worthy to note is that for $\theta_d = 45^o$ the polarization axis rotates with the detuning. This rotation could be quantitatively determined as follows. The polarization axis of detected PL can be found by setting the derivative of the detected PL intensity to zero, where the intensity maximum or minimum occurs. Then we obtain the polarization axis θ^{det} of detected PL:

$$\theta^{\det}(\Delta) = \theta_D + \frac{1}{2}\sin^{-1}\left\{\frac{VL(\Delta)\sin(2\theta_d)}{[1+2VL(\Delta)\cos(2\theta_d)+V^2L(\Delta)^2]^{1/2}}\right\}, \qquad (6)$$

where the parameter $V = \alpha F/P_l$ for clarity. θ^{det} depends on the included angle θ_d as well as the detuning Δ. Figure 5(b) shows the polarization axis of detected PL as a function of detuning for θ_d = 0°, 45° and 90°. A rotation of polarization axis is predicted for θ_d = 45° but no rotation would occur for θ_d = 0° and 90°. We also plot the polarization axes for different V values when θ_d = 45° in Fig. 5(c). It is seen that a larger V value initiates an earlier starting point of rotation because of the stronger Purcell effect. Further discussions on parameter V will be given later.

The above discussions focus on the case of the QD emission coupled to single cavity mode. In fact, for micropillar with circular cross section, there is twofold degeneracy in the fundamental cavity mode. The QD dipole is coupled to both two degenerate modes which are polarized perpendicular to one another. So let us consider a more general case where the degeneracy of fundamental mode is lifted, which occurs in imperfect or elliptical micropillars. In this case, Purcell-enhanced SE rate Γ is given as

#200956 - $15.00 USD Received 7 Nov 2013; revised 30 Dec 2013; accepted 10 Jan 2014; published 15 Jan 2014

$$\Gamma = \gamma_X \left[F_H \cos^2(\theta - \theta_C) L(\Delta_H) + F_V \sin^2(\theta - \theta_C) L(\Delta_V) \right], \quad (7)$$

where F_H and F_V are the respective Purcell factors of two linearly polarized modes. Δ_H and Δ_V are the respective energy detuning between QD and two polarized CMs. Note that the sine square term (rather than cosine square) after F_V arises from the 90° difference between two orthogonal CMs. The general expression for the detected PL of QD coupled to both two modes is written as

$$I_{QD}^{\det} \sim \frac{1-P_l}{2} + P_l \cos^2(\theta - \theta_D) + \alpha_H F_H L(\Delta_H) \cos^2(\theta - \theta_C) + \alpha_V F_V L(\Delta_V) \sin^2(\theta - \theta_C). \quad (8)$$

Here we have taken out the factors independent of the analyzer axis and kept only the polarization-dependent terms. For a circular micropillar, since the fundamental mode is twofold degenerate, so $\Delta_H = \Delta_V$ and $F_H = F_V$. Therefore, cavity-coupled exciton emission rate Γ in Eq. (7) has no polarization dependence. It means that the polarization properties of detected emission will not be modified by the Purcell effect. We now discuss three typical cases of elliptical micropillars with different ellipticity and hence different mode splitting:

(1) $\Delta_H \sim \Delta_V$ and $\Delta_V - \Delta_H << \delta\omega_c$ (our presented case)

The imperfection in micropillars will slightly split the twofold degenerate fundamental mode, which exactly meets our fabricated pillar. Since the mode splitting is rather small compared to the interested coupling regime, the relation $\Delta_H \approx \Delta_V \equiv \Delta$ holds. Thus Eq. (8) reduces to

$$I_{QD}^{\det} \sim \frac{1-P_l}{2} + P_l \cos^2(\theta - \theta_D) + \alpha F_V L(\Delta) \left[\kappa \cos^2(\theta - \theta_C) + \sin^2(\theta - \theta_C) \right], \quad (9)$$

where $\kappa = F_H/F_V$. Again, a zero derivative of detected PL is used to derive the polarization axis. The polarization axis takes the form of Eq. (6) but now with $V = \alpha F_V(\kappa-1)/P_l$. θ_d is explicitly given from the difference of the observed polarization axis between QD and CM at large detuning. The fitting results are plotted in Fig. 6(a). A well-fit for the polarization axis (upper panel in Fig. 6(a)) obtains a V value of 18.2 ± 1.2, where V is the only free parameter of the fit.

Regarding the polarization degree of detected PL intensity, which is defined by $(I_{max}-I_{min})/(I_{max}+I_{min})$, can be derived from Eqs. (6) and (9) as

$$P_l^{\det} = \frac{2\cos^2\left[\theta^{\det}(\Delta) - \theta_D\right] - 1 + VL(\Delta)\left\{2\cos^2\left[\theta^{\det}(\Delta) - \theta_C\right] - 1\right\}}{1/P_l + VL(\Delta)(\kappa+1)/(\kappa-1)}. \quad (10)$$

To determine the unknown κ value, we begin with the case Δ ~0 (on resonance) of Eq. (9). Given that α is large due to the poor coupling between leaky modes and detector, the final term dominates over the former terms. At resonance, the CM emission has a clear dependence on the polarization as shown in Fig. 2(b). Moreover, the polarization properties of CM emission are always preserved even when the detuning is varied. According to the recent understandings of CM emission [26], while entering the Purcell enhancement regime, i.e. our interested detuning region, the CM is weakly coupled to the target QD and emits photons that are mostly contributed from the target QD. That is to say, the polarization dependence of CM emission indicates a polarization dependence of Purcell enhancement experienced by the QD dipole. Therefore, comparing the dominating term in Eq. (9) with the polarization of detected PL emission at Δ ~0, κ can be determined as 1.34. The measured polarization degree compares well with the curve predicted by Eq. (10) when $P_l = 0.4$ as shown in the lower panel of Fig. 6(a).

#200956 - $15.00 USD Received 7 Nov 2013; revised 30 Dec 2013; accepted 10 Jan 2014; published 15 Jan 2014

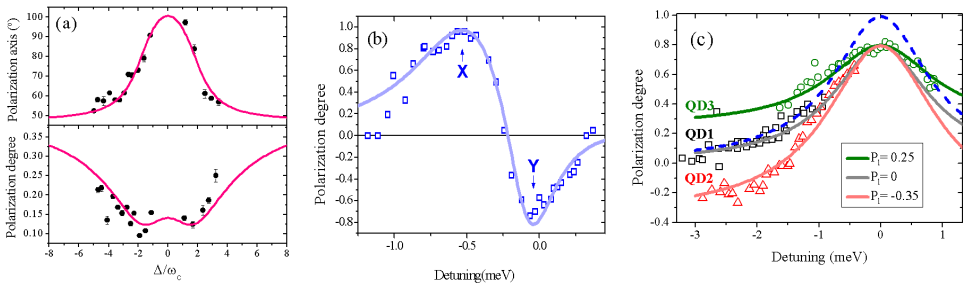

Fig. 6. (a) Calculated curves and our data for the polarization axis (upper) and polarization degree (lower) of detected PL as a function of Δ/ω_c. (b) Comparison of polarization degree between our calculated curve and the measured data taken from [15]. The splitting between X and Y polarized cavity modes is about 500 μeV. (c) Comparison of polarization degree between our calculated curves and the measured data taken from [14]. QD1(black symbol), QD2(red symbol) and QD3(green symbol) respectively own a polarization degree of 0, –0.35 and 0.25 at large detuning. The solid line with corresponding color is calculated with $P_l^{CM} = 0.8$. The blue dashed line is plotted with $P_l = 0$ and $P_l^{CM} = 1$.

(2) $\Delta_H < \Delta_V$ and $\Delta_V - \Delta_H > \delta\omega_c$

For an elliptical micropillar with a small ellipticity, the mode splitting is a few times the cavity linewidth. This case was demonstrated experimentally in [15]. In such micropillars, the polarization of QD emission can be switched between two orthogonal polarizations by changing the coupling of QD with two linearly polarized CMs. In their work, the splitting between two orthogonal polarized modes is about 500 μeV. The studied QD had isotropic polarization, i.e. $P_l = 0$, at large detuning and the polarization degree was defined by $(I_X - I_Y)/(I_X + I_Y)$. According to Eq. (8), the polarization degree of detected PL can be derived as

$$P_l^{\det} = \frac{\alpha_V F_V L(\Delta_V) - \alpha_H F_H L(\Delta_H)}{1 + \alpha_H F_H L(\Delta_H) + \alpha_V F_V L(\Delta_V)}. \tag{11}$$

The index H (V) corresponds to the polarization Y (X) defined in [15]. By exploiting the fact that X polarized mode has a higher quality factor, we obtain the conditions of $\alpha_V F_V > \alpha_H F_H$ and a smaller cavity linewidth for X polarized mode. Giving the parameters with the following values, $\alpha_H F_H = 15$, $\alpha_V F_V = 60$, cavity linewidth of 0.13 for X polarized mode and of 0.15 for Y polarized mode, the curve predicted by Eq. (11) matches the data points measured in [15] as shown in Fig. 6(b). In addition, due to a higher quality factor of X polarized mode, the polarization degree of QD emission at resonance with X polarized mode is higher than that at resonance with Y polarized mode.

(3) $\Delta_H << \Delta_V$ and $\Delta_V - \Delta_H >> \delta\omega_c$

This is the case for micropillars with a large ellipticity. In this case, since the mode splitting is far larger than the cavity linewidth, the mode far from the QD state can be fairly neglected. So we obtain the polarization degree of detected PL of

$$P_l^{\det} = \frac{P_l + \alpha FL(\Delta)}{1 + \alpha FL(\Delta)}. \tag{12}$$

The above formula predicts a highly polarized emission at resonance which is close to unity. The blue dashed line in Fig. 6(c) shows the curve of polarization degree for $P_l = 0$ according to the above formula. The experimental result in [14], in which they studied an elliptical micropillar with the ellipticity of 0.6, is also plotted in Fig. 6(c). The blue dashed line obviously deviates from the data at resonance. We attribute this deviation to a partially polarized CM as observed in [14]. Taking this into account, the detected PL is rewritten as

#200956 - $15.00 USD Received 7 Nov 2013; revised 30 Dec 2013; accepted 10 Jan 2014; published 15 Jan 2014

$$I_{QD}^{\det} \sim \frac{1-P_l}{2} + P_l \cos^2(\theta-\theta_D) + \frac{1}{\xi+1}\alpha FL(\Delta)\left[\cos^2(\theta-\theta_C) + \xi \sin^2(\theta-\theta_C)\right], \quad (13)$$

where the second term in the bracket denotes the PL contribution from orthogonal polarization and ξ is a fraction. The factor 1/(ξ + 1) ensures a normalization of integral over all polarizations for the last term. So the polarization degree is rewritten as

$$P_l^{\det} = \frac{P_l + \alpha FL(\Delta)\cdot P_l^{CM}}{1+\alpha FL(\Delta)}, \quad (14)$$

where P_l^{CM} = (1-ξ)/(1 + ξ) being the polarization degree of CM. Considering a partially polarized CM with P_l^{CM} = 0.8, the polarization degrees of detected PL for QD1, QD2, and QD3 are plotted in Fig. 6(c) by letting P_l = 0.25, 0, and −0.35 and αF = 100, 160 and 150, respectively. It is clear that all calculated curves compare well with the experiments. In short, our analytical model can be used to quantitatively explain all the observed data up to date.

4. Extraction of anisotropic Purcell factors

A further prospect of the PL polarization-resolved measurement on the QD-cavity system is propounded as described below. For the polarization direction of QD orienting an angle with respect to that of CM, it is predicted and demonstrated that a rotation of polarization axis occurs when the coupling of QD with CM is changed. The rotation in the polarization axis of detected PL as seen in Fig. 6 is modeled by Eq. (6) with a given included angle and a fitting parameter V = 18.2 ± 1.2 as mentioned above. According to the formula $V = \alpha F_V(\kappa-1)/P_l$, the Purcell factor F_V can be obtained if α, κ, and P_l are known. Actually, κ and P_l have been determined in the previous section. The value of α, which is the ratio between the collection efficiency of the CM and the leaky mode for the detection system, can be quantitatively determined as follows. We follow the method proposed in [25] and implement pump power-dependent measurements on the investigated micropillar. The integrated PL intensities of the QD against pump power under various detunings are recorded. Note that in this measurement we removed the waveplate and the polarizer in front of the monochromator so that the PL emissions of all the polarizations are entirely collected by the detector. We show the experimental results at the detunings of resonance and far from resonance in Fig. 7. Note that the curve for off resonance case has been rescaled for clarity.

The ratio ε between the total detected PL intensity on resonance and far from resonance is,

$$\varepsilon(\Delta, r) = \frac{I_{QD}^{\det}(0,r)}{I_{QD}^{\det}(\Delta,r)} = \frac{p_X(0,r)}{p_X(\Delta,r)}\frac{1+\alpha F}{1+\alpha FL(\Delta)}. \quad (15)$$

For the pump power well below the one required to saturate the PL emission, the excitonic population is given as $p_X^{below} = r/(\gamma+\Gamma(\Delta))$. As for the pump power well above the saturation, the excitonic population is approximated to be $p_X^{below} = \gamma_{XX}/r$. Comparing the PL intensity with low pump power at resonance and far from resonance, the ratio ε becomes:

$$\varepsilon^{below} = \frac{1+FL(\Delta)}{1+F}\frac{1+\alpha F}{1+\alpha FL(\Delta)}. \quad (16)$$

And the ratio ε for high pump power is:

$$\varepsilon^{above} = \frac{1+\alpha F}{1+\alpha FL(\Delta)}. \quad (17)$$

The Purcell factor can be extracted by dividing Eq. (16) by Eq. (17). Substituting the obtained Purcell factor back into Eq. (17), α is immediately obtained. We thus obtain the Purcell factor

#200956 - $15.00 USD Received 7 Nov 2013; revised 30 Dec 2013; accepted 10 Jan 2014; published 15 Jan 2014

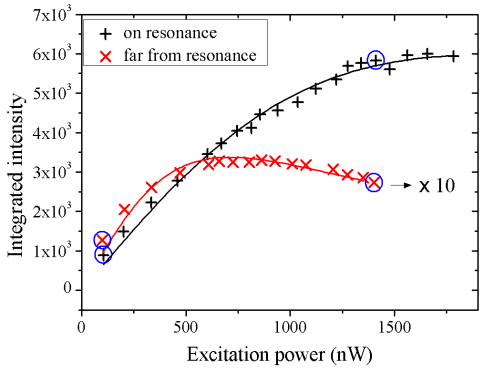

Fig. 7. PL integrated intensity as a function of pump power when on resonance (black cross) and far from resonance (red cross). The data circled are used to extract the ratio α.

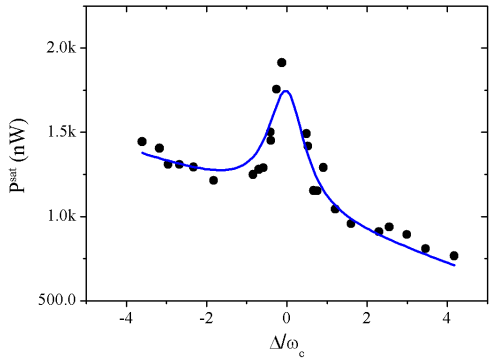

Fig. 8. Saturated pump power as a function of Δ/ω_c. The blue line is plotted with a function of $(1 + FL(\Delta))^{1/2}$.

of 2.3 ± 0.4 and α of 13.8 ± 3.7. Such a large value of α confirms a better collection of photons from the cavity mode than the leaky mode and is comparable to the value obtained in [25]. Since α is determined by the pillar geometry and collection setup (numerical aperture), it should be identical for the pillars of the same diameter measured in the same setup. Therefore, with $P_l = 0.4$ and $\kappa = 1.34$, we obtain $F_V = 1.6 \pm 0.5$ and $F_H = \kappa F_V = 2.1 \pm 0.7$. The difference in Purcell factors between the two polarized CMs could be caused mainly by the spatial mismatch term in Eq. (1) as they have almost the same quality factor.

To further confirm the obtained anisotropic Purcell factors, we perform another measurement which is widely used in QD-micropillar system [2, 25]. The pump power required to saturate the QD emission is recorded as a function of detuning as shown in Fig. 8. We fit the curve with $(1 + FL(\Delta))^{1/2}$ [25] and get the Purcell factor $F = 1.8 \pm 0.2$. It is not surprising that the Purcell factor obtained from this approach lies in between the two anisotropic Purcell factors since the latter approach measures the average one. Note that the error listed here does not consider the intensity fluctuations [25].

At last, we would like to mention another possibility to extract the Purcell factor. Back to aforementioned case that $\Delta_H << \Delta_V$, where the QD is coupled with single cavity mode in an elliptical pillar. The polarization degree of detected PL emission against the detuning is modeled by Eq. (14). For various QDs owning different polarizations, P_l can be explicitly assigned by measuring the polarization of QD emission at very large detuning. Thus the free parameter of this fit is the product of α and F. Evidently we can obtain the Purcell factor with high accuracy if α can be correctly found out. To find α, instead of implementing pump-power dependent measurement, one could possibly compare the cavity emission with the addition of

#200956 - $15.00 USD Received 7 Nov 2013; revised 30 Dec 2013; accepted 10 Jan 2014; published 15 Jan 2014

a pin-hole, which is of the similar size with the micropillar, as close as possible to the micropillar to that with the removal of pin-hole.

5. Conclusion

In conclusion, we propose an analytical model which quantitatively explains the rotation of the polarization angle and the change of the polarization degree of detected PL as a function of detuning, which is observed in our experiment. Our model can be generalized to fit previous works. Moreover, we provide an alternative approach based on analyzing the polarization of detected PL to probe the anisotropic Purcell factors, which is beyond the scope of time-resolved and pump-rate dependent measurements. One should bear in mind that the relatively large error in determining the ratio α is still an obstacle to correctly derive a Purcell factor. A proper way such as the addition of pin-hole to the setup is required to be implemented in order to find correct α.

Acknowledgments

This work was financially supported by NSC and by the ATU Program of MOE in Taiwan. We thank the Center of Nano Science and Technology at NCTU for their equipment support.

#200956 - $15.00 USD Received 7 Nov 2013; revised 30 Dec 2013; accepted 10 Jan 2014; published 15 Jan 2014